Mechanisms of PVDF membrane formation by immersion-precipitation in soft (1-octanol) and harsh (water) nonsolvents

Tai-Horng Young[a], Liao-Ping Cheng[b,*], Dar-Jong Lin[b], Ling Fane[b], Wen-Yuan Chuang[a]

[a]Center for Graduate Institute of Biomedical Engineering, College of Medicine and College of Engineering, National Taiwan University, Taipei 10016, Taiwan
[b]Department of Chemical Engineering, Tamkang University, Taipei, 25137, Taiwan

Abstract

Crystalline PVDF was precipitated, respectively, from water/DMF and 1-octanol/DMF solutions to produce membranes with asymmetric and uniform morphologies. The formation mechanisms of these specific structures were described both in the aspects of thermodynamics (equilibrium phase behavior) and the kinetics (diffusion trajectory). The phase diagrams of the investigated systems indicated the possibility of liquid–liquid demixing or crystallization or both during the immersion-precipitation process. The sequence of these phase separation events, which determined the ultimate membrane structure, was attributed to the kinetic factors. Into this context, a quantitative model describing the immersion-precipitation process was considered. The calculated diffusion trajectory and concentration distribution in the nascent membrane were found to be consistent with the experimental membrane morphologies. Moreover, the precipitation rate of the PVDF solution in water and 1-octanol were examined by the light transmission experiments. The latter results further confirmed the validity of the mass transfer calculations. © 1999 Elsevier Science Ltd. All rights reserved.

1. Introduction

The immersion-precipitation process is nowadays widely used in industry to synthesize polymeric membranes. In this process, a homogeneous polymer solution is immersed in a nonsolvent bath to induce polymeric coagulation. It has long been recognized that precipitation by liquid–liquid demixing gives rise to the observed porous structure of most asymmetric amorphous membranes. However, for crystallizable polymers, precipitation by solid–liquid demixing may take place as well during the immersion process. In this case, the formed membranes exhibit characters from both types of phase demixing. [1,2]. The liquid–liquid demixing process often leads to a cellular morphology whose pores (developed from the polymer-lean phase) are surrounded by a solid polymeric matrix (developed from the polymer-rich phase). In contrast, the solid–liquid demixing occurs in the crystallizable segments of the polymer to form membranes consisting interlinked crystalline particles [3–6]. Because crystallization is a slow process comparing to liquid–liquid demixing, the crystallization-dominated membrane structure is difficult to prepare and its formation mechanism is often overlooked in the literature. Although there are several articles that describe the microporous membrane formation in terms of crystallization during the precipitation process [1–5], the complex precipitation phenomena (including thermodynamics and kinetics) have restricted present-day studies only to the experimental clarification of the relation between membrane preparation conditions and the structures of the precipitated product. In other words, the membrane formation mechanism of the crystalline polymer has not yet been elucidated in detail.

Commercial poly(vinylidene fluoride) (PVDF) membranes have been proved to be useful in biomedical applications [7,8] and in various filtration processes [9,10]. The subject of PVDF membrane formation, however, has rarely been discussed in the literature; particularly the role PVDF crystallization plays during the membrane formation process [11,12]. To have a clear insight into the formation mechanism of PVDF membranes, one often resorts to the phase behavior of the membrane forming system and the kinetics of the immersion process. The phase diagrams of water-DMF-PVDF and 1-octanol/DMF/PVDF systems have been investigated previously

* Corresponding author. Tel.: + 886 2 26215656; fax: + 886 2 26209887.
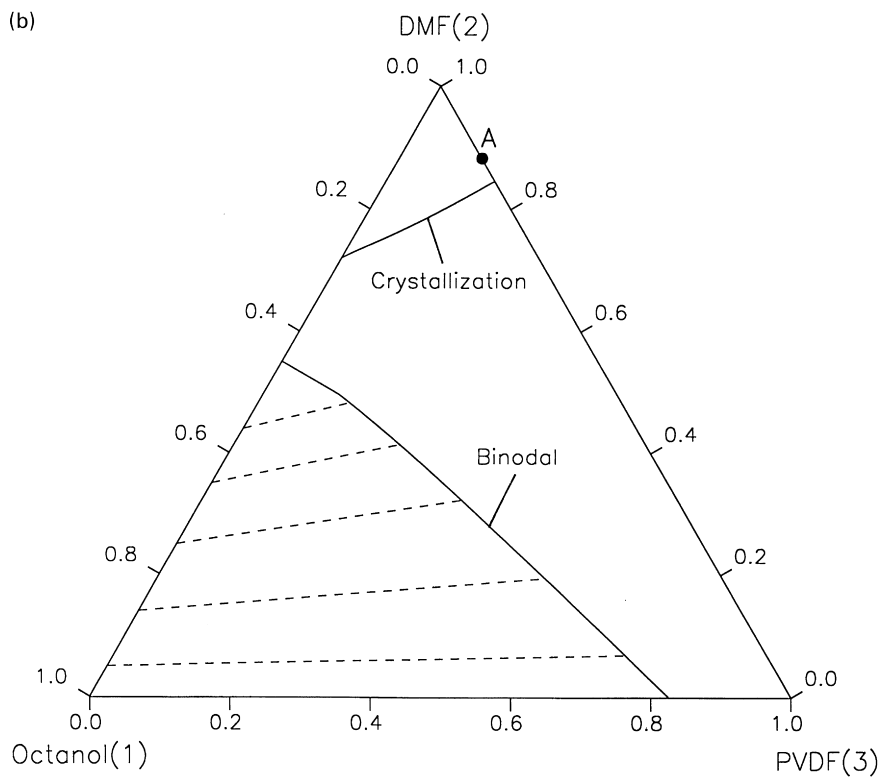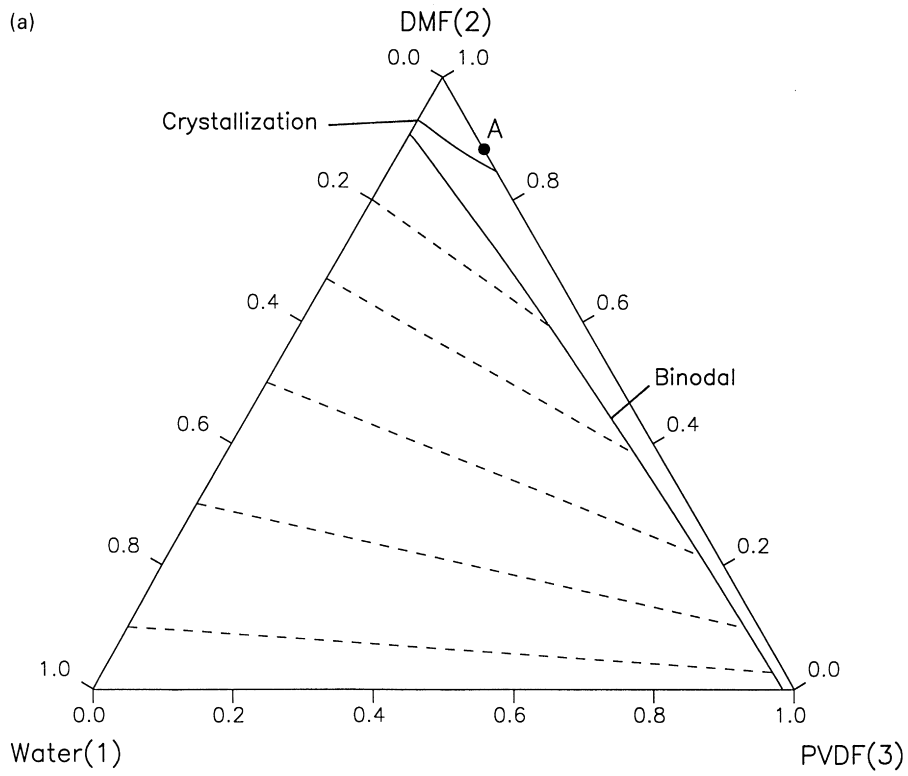*E-mail address:* lpcheng@sigma.che.tku.edu.tw (L.P. Cheng)

Fig. 1. Phase diagrams of two membrane forming systems: (a) water/DMF/PVDF; (b)1-octanol/DMF/PVDF. (--): tie lines of the binodal.

[11,13], as shown in Fig. 1(a) and (b), respectively. These phase diagrams share several common features (e.g.; both the equilibrium crystallization lines are outside the binodal boundaries); but their membrane structures were found to differ markedly. This suggests that phase diagram by itself is not sufficient to explain the formation process of the observed membrane structures in these systems. Obviously, diffusion kinetics of the system plays a role during membrane formation. The first quantitative model that described the immersion-precipitation process for membrane formation was accredited to Cohen et al [14]. During the past three decades, extensive investigations have been performed to unravel the arts behind membrane formation. Various models have emerged ever since; however, most of them were qualitative. Rigorous mathematical treatments came forth only until recently, which were proposed by Reuvers et al [15,16] and by Tsay et al [17]. Unfortunately, these models did not agree with experimental observations in a number of preparation conditions. Later, Cheng [18] published an improved model, which incorporated the essential features of the earlier models. Following Cheng's method, this research developed a mathematical analysis of the formation of crystalline PVDF membranes. The calculated results were found to be consistent with the light transmission measurements and the SEM observations. Based on the analyses of the thermodynamic and kinetic behaviors of the systems, the relation between membrane preparation condition and the obtained membrane structures were discussed.

2. Theory

The immersion-precipitation process has been described as a ternary mass transfer problem previously [18]. The mass transfer equations thus obtained for the membrane solution region are given by

$$\frac{\partial(\phi_1/\phi_3)}{\partial \tau} = \frac{V_1}{D_0} \frac{\partial(\phi_3 L_{11}(\partial \mu_1/\partial \eta) + \phi_3 L_{12}(\partial \mu_2/\partial \eta))}{\partial \eta} \quad (1)$$

$$\frac{\partial(\phi_2/\phi_3)}{\partial \tau} = \frac{V_2}{D_0} \frac{\partial(\phi_3 L_{21}(\partial \mu_1/\partial \eta) + \phi_3 L_{22}(\partial \mu_3/\partial \eta))}{\partial \eta} \quad (2)$$

The equation of continuity for the coagulation bath outside the membrane solution is given by

$$\frac{\partial \phi_1}{\partial \tau} = \frac{M^2}{\delta_c^2} \frac{\partial(D_{12}/D_0)(\partial \phi_1/\partial Y)}{\partial Y}$$

$$+ \frac{1}{D_0}\left(-\frac{3}{8}\frac{V_\infty M^2 \delta_c Y^2}{k\sqrt{z^3}} + \frac{3}{16}\frac{V_\infty M^2 \delta_c^3 Y^4}{k^3\sqrt{z^5}}\right)$$

$$\times \left(\frac{\partial \phi_1}{\partial Y}\right)(f+1) \quad (3)$$

In Eqs. (1)–(3), ϕ_i is the volume fraction of component

i (1: nonsolvent, 2: solvent, 3: polymer). μ_i in is the chemical potential of species i. Eqs. (1)–(3) are transport equations expressed in dimensionless form. The dimensionless time, τ, and the dimensionless distance, η, are defined as: $\tau = D_0 t/M^2$ and $\eta = m/M$, where D_0 is the pre-exponential factor for the diffusion coefficient in Duda's expression [19]. M is the volume per unit area of the initial membrane solution before immersion. The polymer coordinate, m is defined as the volume of polymer between the membrane-bath interface and the position of observation per unit area. L_{jj} ($i, j = 1, 2$) in Eqs. (1) and (2) are coefficients for the phenomenological expressions of diffusional fluxes. δ_c is the thickness of the concentration boundary layer. D_{12} is the mutual diffusion coefficient for the bath liquid. $V\infty$ is the velocity of the free stream. k in Eq.(3) is equal to 4.64 $(\nu/V\infty)^{0.5}$. ν is the kinematic viscosity of the bath liquid. f is a factor which accounts for the effect of mass transfer in the bath direction. Calculated results for the case of $f = 0$ are reported in this work [18]. The detailed derivations of Eqs. (1)–(3) can be found in the literature [18].

3. Experimental

3.1. Materials

PVDF (Kynar 740, Elf Ato Chem) was obtained in pellet form. Dimethylformamide (DMF, Aldrich, HPLC grade) was used as the solvent. Both double distilled-deionized water and 1-octanol (Reidel-de Haen, reagent grade, $d = 0.82$ g/ml) were used as the nonsolvents for the polymer. All materials were used as received.

3.2. Membrane preparation

Membranes were prepared at 25°C using the direct immersion-precipitation method. A homogeneous 22 wt. % PVDF solution (i.e., dope A in Fig. 1) was dispersed uniformly on a glass plate (ca. 300 µm), and then precipitated in nonsolvent to form a laminate. The latter was soaked in ethanol first and then in acetone to remove 1-octanol and residual DMF. The membrane was dried at 45°C and then examined in a scanning electron microscope (SEM, Hitachi S-800) for the top, bottom, and edge views.

3.3. Measurement of precipitation times

Light transmission experiments were performed to obtain the onset and completeness times of phase separation in the immersion-precipitation process. The principle of light transmission experiments is that the light transmittance of the casting solution decreases with the appearance of optical inhomogenities, which can either be induced by liquid–liquid demixing or solid–liquid demixing. Therefore, the time at which the light transmittance begins to decrease is identified as the outset of phase separation, whereas the time at which light transmittance drops to a stable constant value
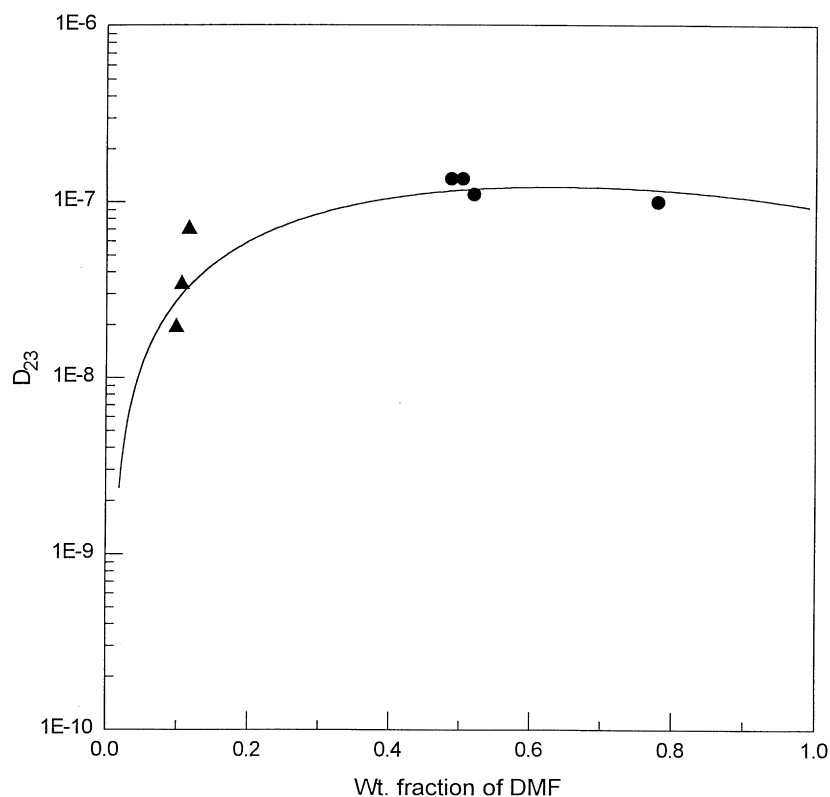
Fig. 2. Mutual diffusion coefficient as a function of solvent weight fraction. (●): measured data for DMF/PVDF binary system. (▲): literature data for acetone/cellulose binary system.

is considered as the completeness of phase separation. To carry out the experiment, a collimated light beam was shone on the membrane solution. The transmitted light intensity was continuously measured by a Si-detector. And a computer was used to store and analyze the intensity profile. Detailed experimental setup and procedures can be referred to a previous publication [18].

3.4. Measurement of the diffusion coefficient

The reflected light differential interference microscope was used to measure the mutual diffusion coefficients between DMF and PVDF in several compositions [13,20]. The results are shown in Fig. 2. In the region where solvent weight fraction is low, the data of acetone-cellulose acetate (e.g., ▲ in Fig. 2) was used to obtain the fitted curve in accordance with Duda's theory [19].

3.5. Computation of the diffusion trajectory

A computer code was used to compute the local concentration of each component in the membrane solution and the bath. The input parameters for calculations are listed in Table 1. The mutual diffusion coefficients between solvent and nonsolvent, D_{12}, were obtained by the Wilke-Chang equation [21]. These diffusion coefficients were transformed into ternary phenomenological coefficients by a procedure described previously [18]. To obtain friction coefficient

between nonsolvent and polymer which is required for L_{ij} calculations, it is assumed that the friction coefficients between polymer and low molecular species (nonsolvent and solvent) are proportional to the volume fractions of the low molecular weight species. Such assumption has also been used elsewhere to yield satisfactory computed results [15–18,22,23]. Various cases corresponding to different preparation conditions were calculated and the results were plotted on the phase diagram to obtain the diffusion trajectories.

Table 1
Parameters for trajectory calculations

	1-octanol bath	Water bath
T (K)	298	298
L (cm)[a]	30	30
$V\infty$ (cm/sec)	10	10
δ_c (m)	0.0652	0.0959
dope thickness (m)	300	200
V_1 (cm^3/mole)	157.194	18
V_2 (cm^3/mole)	77.436	77.436
V_3 (cm^3/mole)	168361	168361
D_{12} (cm^2/sec)	$8.846 \times 10^{-6} - 6.486 \times 10^{-6} \phi_1$	1.7×10^{-5}

[a] L measures the distance between the leading edge and the position of observation. When $L > 30$ cm, concentration boundary layer becomes relatively flat.

4. Results and discussion

4.1. Morphologies of membranes precipitated from water and 1-octanol

To be concise, only two most significant set of results which illustrate the effects of nonsolvent on the membrane structure are discussed here: (a) dope A (Fig. 1) immersed in water (harsh bath) and (b) dope A immersed in 1-octanol (soft bath). The PVDF membrane precipitated from water, as shown in Fig. 3, exhibit an asymmetric structure. Three distinct regions can be identified in this membrane. Near the top surface is a thin dense layer, commonly termed "skin" in the literature. Fig. 3 indicates that this layer is tight and nonporous. Underneath the skin is a region composed of parallel columnar macrovoids which extend to the central part of the membrane. The lower half of the membrane cross section shows a cellular morphology, in which closed pores are enveloped in a polymer mat. All such characteristics can ordinarily be found in amorphous membranes. Since typical morphology from polymer crystallization (i.e., crystalline particles) is not in evidence, the observed membrane structure was derived largely from liquid–liquid demixing. From the phase diagram shown in Fig. 1, however, it appears that during immersion-precipitation mass exchange of solvent and nonsolvent brings the membrane solution into a metastable state initially with respect to solid–liquid demixing, and then with respect to liquid–liquid demixing. In other words, considerations based totally on the phase behavior

will predict a membrane structure controlled by crystallization. Therefore, Fig. 3 suggests that liquid–liquid demixing can precede solid–liquid demixing and dominate the precipitation process even though solid–liquid demixing is favored in a thermodynamical sense.

As the same dope solution (point A in Fig. 1) was immersed in 1-octanol, the morphology of the formed membrane differs dramatically from that shown in Fig. 3. Fig. 4 presents a uniform microporous structure composed of spherical particles (1.5 μm, dia.) of approximately the same size. Other dimensions of this membrane have largely identical structure and are therefore not shown here. Such structure represents a crystallization-dominated precipitation situation, wherein all crystalline particles were nucleated and grown in a similar concentration field and finally fused together to form a bi-continuous structure [23].

To explain the formation mechanism of the previously mentioned asymmetric or particulate structure, one normally has to consider both the thermodynamic (phase behavior) and the kinetic (mass transfer) aspects of the formation process. The phase diagrams in Fig. 1(a) and (b) indicate that there is a wider gap between the crystallization line and the binodal for the 1-octanol/DMF/PVDF system than for the water/DMF/PVDF system, and that the liquid–liquid demixing boundary of the former system is much smaller than that of the latter system. This indeed suggests a more favorable condition for PVDF to precipitate into a crystallization orientated structure in 1-octanol than in water. However, Fig. 1 also indicates that the crystallization
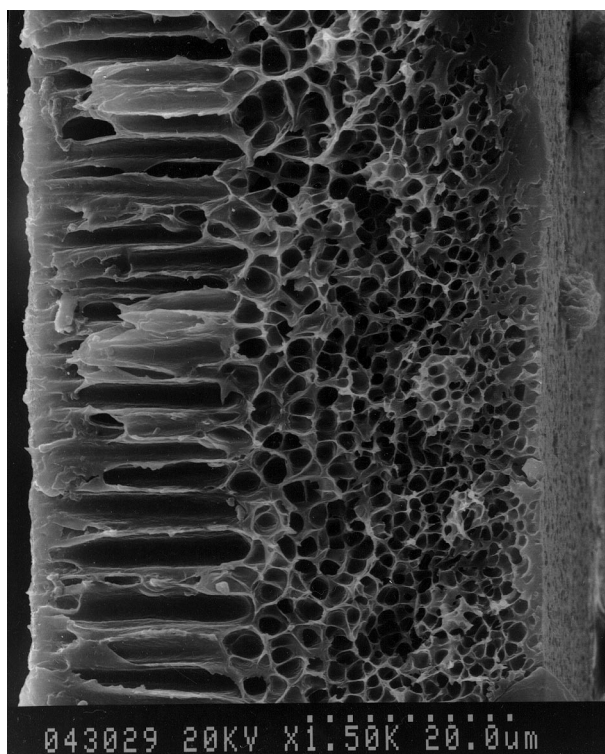

Fig. 3. SEM photomicrograph showing the cross section of the membrane prepared by immersing dope 'A' (Fig. 1) in water.
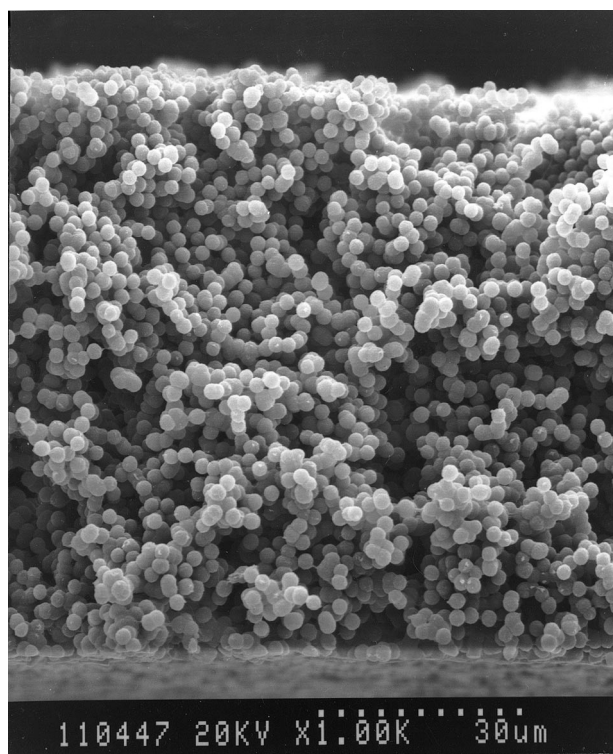

Fig. 4. SEM photomicrograph showing the cross section of the membrane prepared by immersing dope 'A' (Fig. 1) in 1-octanol.
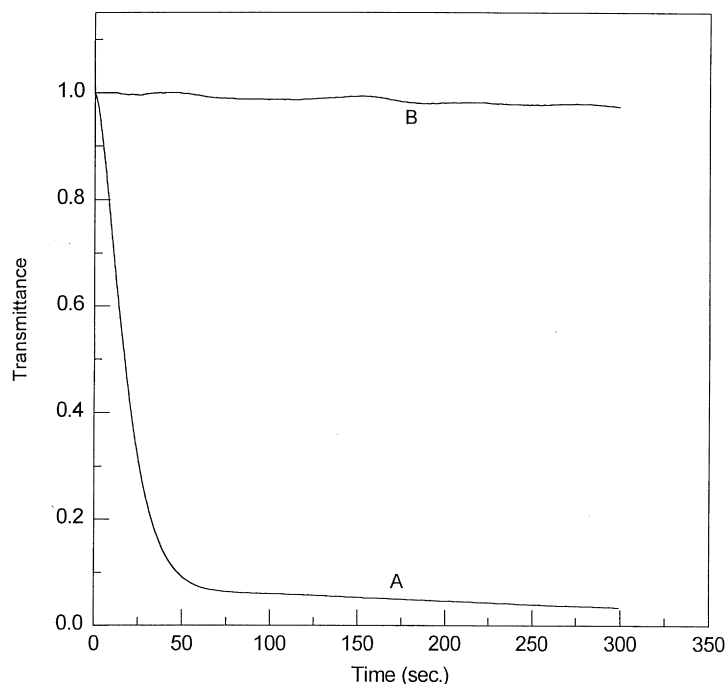
Fig. 5. Light transmittance during immersion of PVDF solutions into different baths. A: water bath. B: 1-octanol.

boundary must be entered before there is any chance for liquid–liquid demixing to occur, irrespective of immersing in water or 1-octanol. Therefore, the time needed to initiate crystallization (normally slow because of nucleation and growth) relative to that for membrane solution to enter the binodal also affects the sequence of the two-phase separation processes and thus the membrane morphology. In other words, the kinetic factors play an important role in the membrane formation process. It is possible that the diffusional mass transfer of solvent and nonsolvent is so fast that before the nucleation process of crystallization, the binodal boundary has been crossed and liquid–liquid demixing takes place rapidly to yield an asymmetric morphology, as depicted in Fig. 3. In contrast, if the mass transfer is slow (e.g., immersing in a soft bath), crystallization occurs prior to liquid–liquid demixing and a "particulate" morphology results, as shown in Fig. 4. In the discussion that follows, the kinetical viewpoint of the membrane formation process will be based upon the light transmittance measurements and the diffusional path calculations. These results together with the phase diagrams will illustrate clearly the causes of the marked differences in membrane structures prepared in water and in 1-octanol.

4.2. Precipitation times of membranes precipitated from water and 1-octanol

Light transmission experiments were carried out to follow the course of the precipitation process. The results are presented in Fig. 5 in the form of transmittance profiles.

An instantaneous demixing is observed in the case of immersing the dope in water. Curve 'A' shows that the light transmittance drops off immediately after dope-bath contact and the light transmittance arrives at a constant stable value at ca. 50 s. Therefore, the structure of the membrane were set in shortly after the much faster process of nonsolvent–solvent exchange. In such a short time frame, no polymer crystallization could possibly occur. Instead, the intrusion of nonsolvent brought quickly to the membrane solution into the binodal region in which liquid–liquid demixing initiated and dominated the membrane precipitation process, thereby forming the asymmetric structure shown in Fig. 3. The situation reversed when 1-octanol was used as the nonsolvent. Curve 'B' in Fig. 5 indicates a delayed type of demixing [16]. The light transmission intensity decreased by less than 2% after immersion for ca. 300 s. Although this small change in intensity may be caused by the proximity of refractive indices between the nascent membrane and the bath liquid, the membrane solution in fact becomes a soft gel and could be removed from the glass plate at 3 min. after immersion. In this slow precipitation case, the exchange of nonsolvent and solvent was very slow, and hence nucleation of polymer crystallites within the membrane solution prior to liquid–liquid demixing became feasible. As will be shown later by diffusion trajectory calculations, liquid–liquid demixing will not take place even at 3 min. after contact of the dope and the bath. Therefore, crystallization dictated the precipitation process to form the "particulate" morphology i.e., shown in Fig. 4.
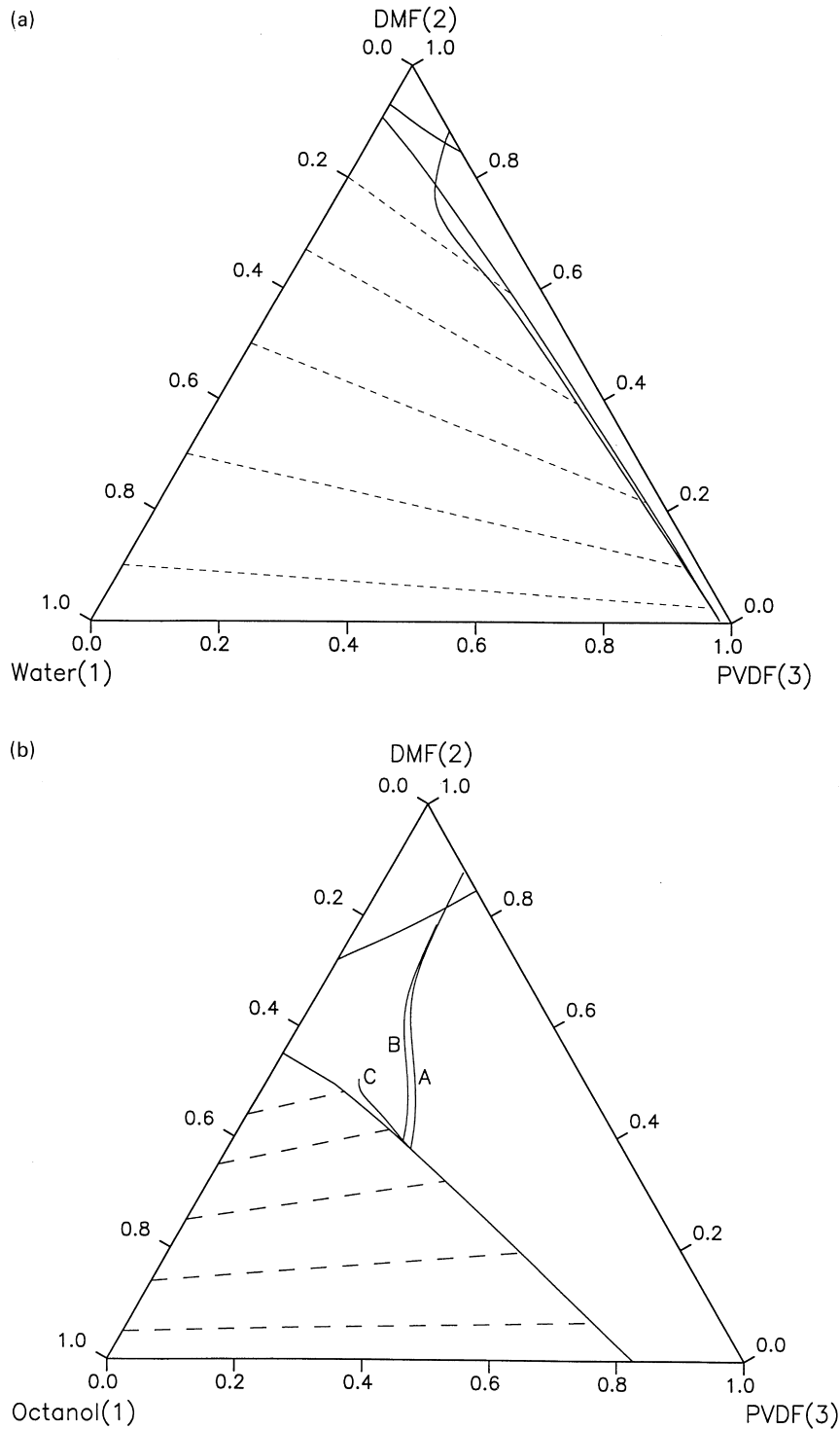
Fig. 6. Calculated diffusion trajectories for immersing dope 'A' into different baths. (a) water bath. (b) 1-octanol bath, trajectory 'A': 60 s., trajectory 'B': 180 s., trajectory 'C': 540 s.,

4.3. Diffusion trajectories of membranes precipitated from water and 1-octanol

The mass transfer process during immersion-precipitation before the occurrence of phase separation was modeled as a ternary diffusion problem. The calculated diffusion trajectories and concentration profiles are shown, respectively, in Figs. 6 and 7. The dope solution contained 20 wt. % PVDF and the bath was either water or 1-octanol. The trajectories represent the compositions of each component in the membrane solution at different times after immersion; they are plotted on a ternary phase diagram as
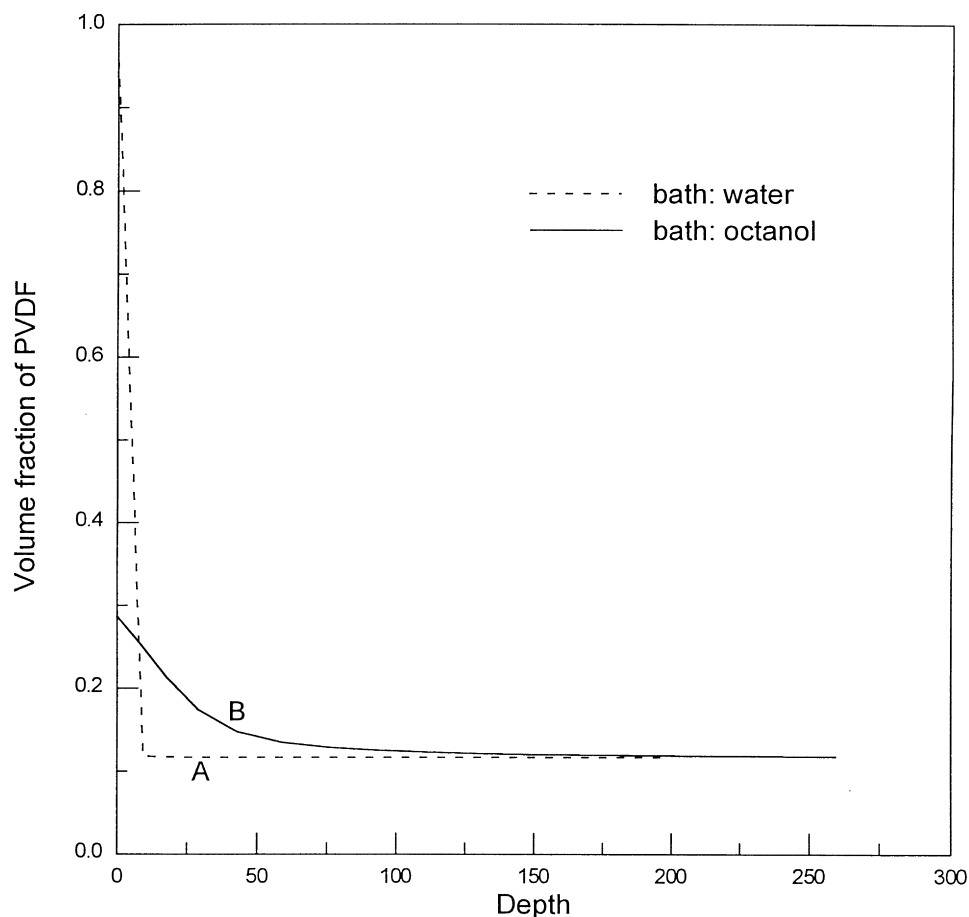
Fig. 7. Calculated polymer volume fraction profiles for immersing dope 'A' into different baths. Curve 'A': water bath (1. s.), Curve 'B': 1-octanol bath (180 s).

shown in Fig. 6. The interfacial composition of the membrane solution is located on the binodal, in accordance with the assumed equilibrium boundary condition. For the case of immersing the dope in water, Fig. 6(a) indicates that the diffusion trajectory crosses the binodal immediately at contact of the dope with the bath. This agrees with the precipitation time observed in the light transmission experiment. Such type of precipitation was coined "instantaneous demixing" by Reuvers et al. [16]. The membranes thus formed usually feature a tight skin and a cellular sublayer, and in many cases the macrovoids are prevalent in the membrane cross section [16,23–26]. Fig. 3 provides evidence for this latter structure.

The volume fraction of polymer along the membrane cross section when the trajectory first enters the binodal is shown as curve 'A' in Fig. 7. The composition of the membrane-bath interface is located on the y-axis (depth = 0) and the composition of the bottom surface is on the other end of the concentration profile. Curve 'A' indicates a pronounced high polymer concentration near the interfacial region followed by a constant low concentration all the way toward the bottom surface. The high interfacial polymer concentration brought this region rapidly into a state

where vitrification took place and the structure froze. Hence, the skin layer was very hard and stiff so as to preclude any possibility of microporous regions near this surface. Although the diffusion trajectory alone does not predict a liquid–liquid demixing dominated precipitation process in the porous region underneath the skin, the SEM in Fig. 3 and the light transmission experiment both indicate such a dominance. In such a short time domain, it appears that the normally sluggish crystallization process was not likely to commence earlier than liquid–liquid demixing. Concerning the formation of macrovoids, it is beyond the scope of the current work. However, the steep concentration gradient, as shown in Fig. 6, formed instantly at contact with the bath indeed suggests a favorable condition for macrovoid formation [16,23–26].

In contrast to the instant demixing case, as 1-octanol was used as the coagulation bath, mass transfer between solvent–nonsolvent became laggard and precipitation was delayed (see Fig. 5). As shown in curve 'C' of Fig. 6(b), the diffusion trajectory enters the binodal very slowly at ca. 540 s after immersion. This is much longer than the observed precipitation time. Because of such deferral of the liquid–liquid demixing process and also because the

membrane solution was highly supersaturated with respect to crystallization within this time scale, nucleation and growth of polymer crystallites took place and dominated throughout the precipitation process. This is consistent with the morphology of the membrane presented in Fig. 4. The cellular-like pores are not observable and the membrane demonstrated a microporous structure packed by spherical crystallites. The calculated polymer concentration in the membrane solution at 180 s. is shown as curve 'B' in Fig. 7. Instead of a sharp increase in polymer concentration close to the top surface in curve 'A', curve 'B' shows a steady and small decrease in ϕ_3. Because of the small difference in ϕ_3 across the membrane solution, the particles in the membrane were thought to emerge from individual PVDF nuclei formed roughly simultaneously. These nuclei then grew radially until their fronts impinged and then joined with adjacent particles to form a skinless and microporous structure which was confirmed by the SEM shown in Fig. 4.

5. Conclusion

Considerations based totally on equilibrium thermodynamic were not adequate to explain the structural difference of the membranes prepared from water-DMF-PVDF and 1-octanol-DMF-PVDF systems. Because PVDF is highly crystalline, it may precipitate both by liquid–liquid demixing and crystallization. From the kinetic point of view, crystallization nucleation depends much on the degree of supersaturation. Therefore, even though the membrane solution enters the crystallization zone before the binodal, crystallization probably will not take place because of its competition with the liquid–liquid demixing process. When water was used as the nonsolvent, the diffusion trajectory crossed the crystallization line without rapid crystallization as a result of instant liquid–liquid demixing. This resulted in a typical asymmetric membrane. However, when 1-octanol was used as the nonsolvent, mass transfer became slow and liquid–liquid demixing was suppressed. The resultant membrane exhibited a crystallization-controlled morphology. Therefore, in order to understand the membrane formation mechanism of a system involving a crystalline polymer, in addition to the equilibrium phase behavior, the diffusion kinetics has to be considered as well.

References

[1] Cheng LP, Dwan AW, Gryte CC. J Polym Sci, Polym Phys 1995; 33:211.
[2] Young TH, Lai JY, Yu WM, Cheng LP. J Membr Sci 1997;128:55.
[3] Lloyd DR, Kinzer KE, Tseng HS. J Membr Sci 1990;52:239.
[4] Bulte AMW, Folkers B, Mulder MHV, Smolders CA. J Appl Polym Sci 1993;50:13.
[5] van de Witte P, Esselbrugge H, Dijkstra PJ, van de Berg JWA, Feijen J. J Polym Sci: Polym Phys 1996;34:2569.
[6] Aubert JH. Macromolecules 1988;21:3468.
[7] Guenard V, Valentini RF, Aebischer P. Biomaterials 1991;12:259.
[8] Chen H, Soldani G, Galletti PM, Goddard M. ASAIO J 1992;38:201.
[9] Grandien JD. United States Patent 4203847, 1977.
[10] Grandien JD. United States Patent 4203848, 1977.
[11] Cheng LP, Young TH, Fang L, Gau JJ. Formation of particulate microporous polyvinylidene fluoride) membranes by isothermal immersion precipitation from the 1-octanol/dimethlformamide/poly (vinylidene fluoride) system. Polymer, in press.
[12] Soh YS, Kim JH, Gryte CC. Polymer 1995;36:3711.
[13] Dwan AW. Doctoral Dissertation, Columbia University, 1995.
[14] Cohen C, Tanny GB, Prager SJ. Polym Sci, Polym Phys 1979;17:17–477.
[15] Reuvers AJ, van den Berg JWA, Smolders CA. J Membr Sci 1987;34:45.
[16] Reuvers AJ, Smolders CA. J Membr Sci 1987;34:45.
[17] Tsay CS, McHugh AJ. J Polym Sci, Polym Phys 1990;28:1327.
[18] Cheng LP, Dwan AH, Soh YS, Gryte CC. J Polym Sci, Polym Phys 1994;32:1413.
[19] Vrentas JS, Duda JL. AIChE J 1982;28:279.
[20] Cheng LP, Dwan AH, Gryte CC. J Appl Polym Sci 1995;57:563.
[21] Reid RC, Prausnitz JM, Sherwood TK. The properties of gases and liquids. 3rd ed.. New York: McGraw-Hill, 1997.
[22] Cheng LP, Dwan AW, Gryte CC. J Polym Sci, Polym Phys 1995;33:223.
[23] Cheng LP, Young TH, You WM. J Membr Sci 1998;145:77.
[24] Strathmann H. Production of microprobes Media by Phase Inversion Process. In Lloyd DR, editor. Material science of synthetic membrane. ACS Symposium Series, 1985.
[25] Smolders CA, Reuvers AJ, Boom RM, Wienk IM. J Membr Sci 1992;73:259.
[26] McKelvey SA, Koros WJ. J Membr Sci 1996;112:29.